Theor Chim Acta (1989) 75: 195–222

Theoretica Chimica Acta

Electronic structure of azidomyoglobin and associated magnetic and hyperfine properties*

Santosh K. Mishra, J. N. Roy, K. C. Mishra, and T. P. Das

Department of Physics, State University of New York at Albany, Albany, NY 12222, USA

(Received April 6/Accepted June 6, 1988)

The electronic structure of azidomyoglobin has been investigated for understanding the observed magnetic and hyperfine properties of this system. The results of our investigation show that a configuration with five electrons in d-like molecular orbital states, as in the case of ferricytochrome c but unlike nitrosylhemoglobin, provides a satisfactory explanation of the observed strongly rhombic g-tensor, the ^{57m}Fe quadrupole splitting from Mössbauer measurements and the porphyrin ^{14}N quadrupole interactions. For the magnetic hyperfine interactions of the ^{57m}Fe and porphyrin ^{14}N nuclei, there are significant differences between theory and experiment. For the ^{57m}Fe nucleus, after incorporating the influence of spin-orbit effects, which leads to unquenching of the orbital angular momentum through admixture of excited state configurations to the ground state one, very good agreement is found with single crystal Mössbauer data. For ^{14}N hyperfine interactions associated with the pyrrole group however, where spin-orbit effects are expected to be much less pronounced, the theoretical values of the hyperfine constants are found to be less than a fifth of those derived from ENDOR measurements. It is suggested that the difference between theory and experiment could be bridged through incorporation of exchange polarization contribution to the ^{14}N hyperfine interaction from the sizeable valence electron spin density (about 65 per cent of the total) on the iron atom. The need for additional experimental measurements is pointed out, among them ENDOR measurements to determine the hyperfine properties of the azide nitrogens for which the end nitrogens are predicted from the present work to have sizeable magnetic hyperfine constants (about −10 MHz).

Key words: Electronic structure—Hyperfine properties—g-Tensor—Myogobin azide

* This work was supported by National Institute of Health Grant HL15196

1. Introduction

Recent theoretical studies [1] on electronic structures of low spin paramagentic ($S = 1/2$) ferric hemoglobin derivatives to interpret available hyperfine data on these systems have shown that the nature of the unpaired spin orbital, and hence the spin distribution, depends sensitively on the sixth ligand. Thus, in nitrosylhemoglobin [1a] and deoxycobaltglobin [1b], the unpaired spin electron was found to be in a d_{z^2}-like orbital. In ferricytochrome c [1c] and oxycobaltglobin [1b], on the other hand, the theoretical analysis and observed ^{14}N hyperfine data lead to the assignment of the unpaired spin orbital to a mixture of d_{xz} and d_{yz}-like states. In the present work we have studied the azidomyoglobin (AzidoMb) system, both to examine the nature of the unpaired spin orbital when the sixth ligand is an azide group, and also to attempt to explain the observed hyperfine data [2, 3] and g-tensor [4] in this system. Our investigation supports the assignment of the unpaired spin orbital to a state which, as in the case of ferricytochrome c, is a mixture of d_{xz} and d_{yz}-like atomic orbitals and suggests the need for additional hyperfine data to verify this assignment. AzidoMb was also of interest to study because of the availability of ^{14}N hyperfine data [2], indicating differences between AzidoMb and AzidoHb and between α and β chains of AzidoHb, which provide insight into the influence of neighboring groups on the protein chains on the unpaired spin distribution on the heme system. An understanding of this influence requires a good knowledge of the absolute spin distribution of any one of these systems, which we have chosen as AzidoMb in our work.

Section 2 deals with the theory of the electronic structure and hyperfine interaction and g-tensor investigations on AzidoMb. Since the self-consistent charge extended Hückel (SCCEH) procedure [5] used in our work has been extensively discussed in the literature, only a brief description of this procedure will be given to facilitate the discussions in subsequent sections. The geometry for the molecule used in our investigations will also be discussed in this section, as well as the proecdure for the calculation of the ^{57m}Fe and ^{14}N magnetic and nuclear quadrupole hyperfine interactions. Section 3 will present our results and comparison with experimental hyperfine [2, 3] and g-shift data [4] and conclusions regarding the nature of the unpaired spin electron. Additional theoretical and experimental investigations that can further enhance our understanding of the electronic structure of AzidoMb will be discussed there.

2. Procedure

2.1. *Structural description of* AzidoMb

The model system used as the prototype for AzidoMb for our electronic structure investigations is shown in Fig. 1. As in earlier investigations [1] on other heme systems, we have assumed four-fold symmetry for the porphyrin ring and replaced the side-chains of the pyrroles by hydrogen atoms. The iron atom was assumed to be located on the porphyrin plane, the positions of the atoms in the fifth and sixth ligands relative to the iron being taken from X-ray data [6]. The plane of the porphyrin was taken as the XY plane with the Y and X axes passing through

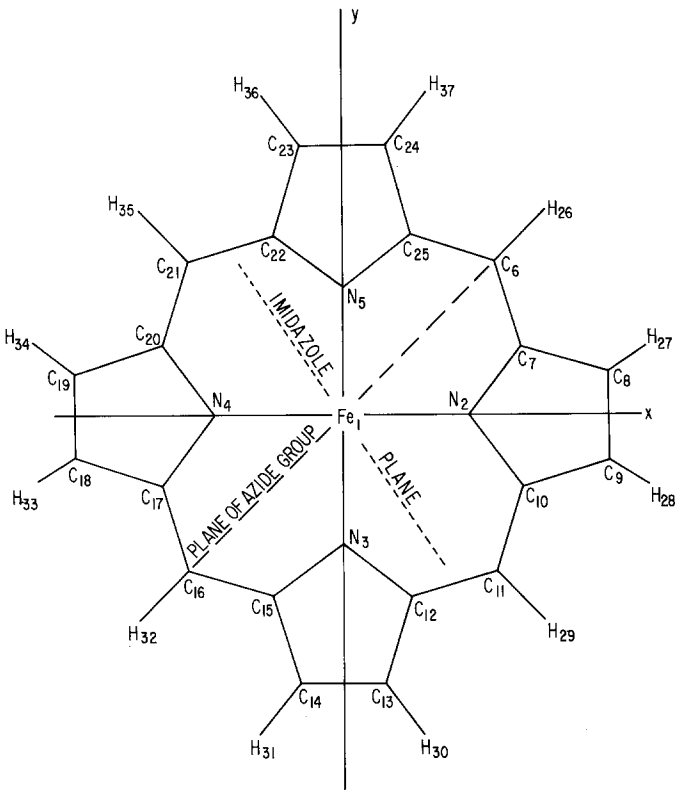

Fig. 1. Model system used for AzidoMb. The atoms are numbered according to the order they appear in Table 1. The azide group is inclined at 69° to the Z-axis, which is perpendicular to the heme plane, the relative orientations of the azide and imidazole planes being as indicated. The distance between Fe and the nearest nitrogen of the azide group is 2.1 Å

(N_3, N_5) and (N_4, N_2) atoms respectively. The fifth ligand was a protonated imidazole, its plane being taken [6] as that formed by the Z-axis and a line on the XY plane inclined at 61° to the X-axis as shown in Fig. 1. The azide group (N_3^-) forms the sixth ligand, being linear and inclined [5] to the Z-axis at 69°. This group and the heme normal form a plane which passes through two methine carbon atoms opposite to each other as shown in Fig. 1 and makes an angle of 64° with respect to the plane of the imidazole. The N_α atom of the azide group is located at a distance of 2.1 Å from the Fe atom, the separation between successive nitrogen atoms of the N_3^- group being 1.15 Å.

2.2. Electronic wave-functions

A number of different procedures have been used in the literature for the study of electronic structures of heme compounds and hemoglobin derivatives. Among these are the crystal field procedure [7], the self-consistent charge extended Hückel (SCCEH) procedure [5, 8, 9], the Pariser-Parr-Pople procedure [10], the

multiple scattering-X_α procedure [10, 11] and the Hartree–Fock procedure [12]. In our investigations on magnetic and hyperfine properties of heme systems [1, 5b, 9, 13], we have been using the SCCEH procedure, especially for high-spin ferric heme systems. The SCCEH procedure has been successfully used [13] for explaining the magnetic hyperfine interactions of ^{57m}Fe, ^{14}N and ^{1}H nuclei as well as the zero-field splitting in the high spin ferric systems and the ^{57m}Fe nuclear quadrupole interaction in oxyhemoglobin [14, 15]. In the present work, as well as in our earlier investigations of low spin ferric heme systems, we have continued to use the SCCEH procedure. As we have remarked in Sect. 3 that it would be useful to have investigations of AzidoMb by other procedures in the future.

Detailed descriptions of the SCCEH procedure utilized to obtain the electronic wave functions in AzidoMb are available in the literature [5]. We shall discuss only a few of the features of the technique that are important for the consideration of the hyperfine properties of interest to us here. The molecular orbitals ϕ_μ, in this procedure, are expressed as a linear combination of atomic valence orbitals χ_i in the variational form:

$$\phi_\mu = \sum_i C_{\mu i}\chi_i. \tag{1}$$

The coefficients $C_{\mu i}$ are obtained by solving the linear equations,

$$\sum_i C_{\mu i}(\mathcal{H}_{ij} - \varepsilon_\mu S_{ij}) = 0 \tag{2}$$

leading to the secular equation:

$$\mathrm{Det}|\mathcal{H}_{ij} - \varepsilon_\mu S_{ij}| = 0, \tag{3}$$

where $\mathcal{H}_{ij}$ and S_{ij} are the Hamiltonian and overlap matrix elements, and ε_μ refers to the molecular orbital energy. The Hamiltonian matrix elements $\mathcal{H}_{ij}$ are obtained [5] using semiempirical relations involving the ionization energies form the atoms and corresponding ions in the molecule, the overlap matrix elements S_{ij}, and the charges on the atoms in the molecule. The latter are related to the coefficients $C_{\mu i}$ through the Mulliken relation [16], which brings in charge consistency to this procedure.

2.3. g-Tensor

The g-tensor in hemoglobin derivatives have usually been analyzed [17] in the literature using a crystal field approach. This approach uses for the electronic wave-functions the pure 3d functions of iron and incorporates the influence of the ligands through the splitting of the 3d energy levels. The splittings are adjusted to fit the components of the g-tensor using a perturbation approach, involving the combined effects of spin-orbit interaction and the interaction between the orbital and spin angular momentum of the electrons and the applied magnetic field. The splittings obtained in this manner provide useful insight into the nature of the iron-ligand interactions. In the present work, we are however interested in subjecting our calculated electronic structure and associated spin-density for the AzidoMb system to a detailed test by attempting *ab initio* explanations of its

observed hyperfine and magnetic properties. Therefore, rather than attempting to fit observed g-tensor data [4] through adjustment of the energy denominators, we shall use a perturbation approach based on the molecular orbital energies and wave-functions obtained from our investigations and compare the theoretical g-tensor components with experimental data. The perturbation procedure that we shall use is presented in detail elsewhere [18]. It essentially equates the matrix elements of the Spin-Hamiltonian term

$$\mathcal{H}_{\text{spin}} = \beta \boldsymbol{S} \cdot \boldsymbol{g} \cdot \boldsymbol{H} \tag{4}$$

over the many-electron wave-function for the molecule in question to the corresponding matrix elements involving one order each in the spin-orbit Hamiltonian $\mathcal{H}_{\text{SO}}$ and the Zeeman Hamiltonian $\mathcal{H}_{\text{m}}$ given respectively by:

$$\mathcal{H}_{\text{SO}} = \sum_{i,\text{A}} \xi_{\text{A}} \boldsymbol{l}_{i\text{A}} \cdot \boldsymbol{s}_i \tag{5}$$

and

$$\mathcal{H}_{\text{M}} = \beta \boldsymbol{H} \cdot \left[\sum_i \boldsymbol{l}_i + g_e \sum_i \boldsymbol{s}_i \right]. \tag{6}$$

In Eqs. (4) through (6), β is the Bohr magneton, $\boldsymbol{H}$ the applied field, ξ_{A} the spin-orbit constant for a specific atom A, $\boldsymbol{l}_i$ the orbital angular momentum for the ith electron ($l_{i\text{A}}$ referring to angular momentum with respect to nucleus A as origin), $\boldsymbol{s}_i$ the spin of the ith electron, $\boldsymbol{S}$ the total spin of the molecule and g_e the free electron g-factor, 2.0023. By this procedure one obtains, for the $(\alpha\beta)$ component of the g-tensor [19],

$$g_{\alpha\beta} = g_e \delta_{\alpha\beta} \pm 2 \sum_n \sum_{ijkl} C^0_{\mu i} C^n_{\nu j} C^n_{\nu k} C^0_{\mu l} \frac{\langle x_i | l_\alpha | x_j \rangle \langle x_k | \xi_{\text{A}} l_{\text{A}\beta} | x_l \rangle}{\varepsilon_\mu - \varepsilon_\nu}. \tag{7}$$

In Eq. (7), the superscripts (0) and (n) refer to the ground and excited states of the whole molecule, the latter involving an excitation of an electron from an occupied moleclar orbital state μ to an empty state ν. The positive sign in Eq. (7) corresponds to having the unpaired spin (referred to as up spin) electron excited to a higher empty state while the negative sign corresponds [17, 18] to an excitation of an electron in an occupied state with down spin to the down spin unpaired state which is unoccupied in the ground state of the whole molecule. The ε_μ and ε_ν refer to the one-electron energies for the molecular orbital states μ and ν, while the $C_{\mu i}$ and χ_i have the same meaning as in Eq. (1).

2.4. Nuclear quadrupole and magnetic hyperfine constants

The Spin-Hamiltonian [2, 20] which is utilized to interpret experimental data from magnetic resonance or Mössbauer measurements, can be written in the general form

$$\mathcal{H}_{\text{spin}} = \mu_B \boldsymbol{H} \cdot \boldsymbol{g} \cdot \boldsymbol{S} - \sum_N [\gamma_N \hbar \boldsymbol{I}_N \cdot \boldsymbol{H} + \boldsymbol{I}_N \cdot \boldsymbol{A} \cdot \boldsymbol{S} + \boldsymbol{Q}_N \cdot (\nabla \boldsymbol{E})_N] \tag{8}$$

where the first term represents the Zeeman interaction between the electron spin and the applied field, considered already for the g-tensor discussed in the preceding subsection. The second term represents the Zeeman interaction between the nuclear magnetic moments in the molecule and the applied magnetic field, the third term the magnetic hyperfine interaction between the nuclear magnetic moments and the electronic spin of the molecule and the fourth term the quadrupole interactions of the nuclei with the electrons and nuclear charges in the molecules, $\boldsymbol{Q}_N$ being the quadrupole moment tensor for the Nth nucleus and $(\nabla \boldsymbol{E})_N$ the field-gradient tensor at this nucleus. In our work here, we shall be analyzing the nuclear quadrupole and magnetic hyperfine interactions of both ^{57m}Fe and ^{14}N nuclei which are available respectively from Mössbauer and electron-nuclear double resonance (ENDOR) methods.

2.4.1. Quadrupole interaction. We shall consider the nuclear quadrupole interactions first. For the interpretation of ^{57m}Fe quadrupole splittings from Mössbauer data [3], we need to consider the last term in Eq. (8) in terms of the principal components of the field-gradient tensor $\nabla \boldsymbol{E}$. The corresponding expression for a particular nucleus is given by [21]

$$\mathcal{H}_Q = \frac{3e^2qQ}{4I(2I-1)}\left[\left(I_{z'}^2 - \frac{I(I+1)}{3}\right) + \frac{\eta}{3}(I_{x'}^2 - I_{y'}^2\right], \tag{9}$$

where $q = V_{z'z'}$ represents the largest component of the field gradient tensor in the principal axis system and η is the conventional asymmetry parameter given by

$$\eta = \left|\frac{V_{x'x'} - V_{y'y'}}{V_{z'z'}}\right|, \tag{10}$$

with $|V_{z'z'}| > |V_{y'y'}| > |V_{x'x'}|$ so that η lies between 0 and 1. The frequency difference between the $M_I = 3/2$ and $M_I = 1/2$ sublevels of the excited $I = 3/2$ state ^{57m}Fe of the iron nucleus is given by:

$$\nabla\nu = \frac{e^2qQ}{2h}\sqrt{1+(\eta^2/3)} \tag{11}$$

in Hz. For the evaluation of the principal components $V_{x'x'}$, $V_{y'y'}$ and $V_{z'z'}$ of the electric field gradient tensor, the components of the latter, both diagonal and off-diagonal, were first evaluated in the molecular axes system (X, Y, Z) in Fig. 1 and are given in the local approximation [22], which has been found to be satisfactory in other heme systems, by

$$V_{ij} = \sum_{\mu}\left\langle \phi_\mu \left| \frac{3\chi_i\chi_j - r^2\delta_{ij}}{r^5} \right| \phi_\mu \right\rangle, \tag{12}$$

with i and j running over (X, Y and Z) and the ϕ_μ referring to all the occupied paired orbitals with up and down spin and unpaired orbitals. This expression should be multiplied by a Sternheimer shielding factor but in view of the fact that this factor has been found [23] to be rather small, namely of the order of

0.05, it has been neglected in Eq. (12). Once the non-diagonal tensor with components V_{ij} have been obtained, the principal components $V_{i'j'}$ and principal axes may be determined by the appropriate diagonalization procedure.

For the ^{14}N nuclei, the quadrupole interaction data, obtained experimentally [2] by the ENDOR technique, involves only the field-gradient tensor component $V_{z'z'}$ where z' refers to the direction for the maximum component of the g-tensor. These components $V_{z'z'}$ for the various ^{14}N nuclei will be evaluated from appropriate combinations of the components V_{ij} in Eq. (12) for the molecular axes system.

2.4.2. Magnetic hyperfine interaction. The magnetic hyperfine interaction tensor arises from the contact and dipolar interactions between the nuclear magnetic moment and the electronic spin magnetic moments. The orbital contributions from the electrons is usually considered to be absent because of the quenching of the orbital angular momentum in the molecule. There can of course be a finite contribution of this type due to the unquenching effect produced by spin-orbit interaction which leads to the tensor character of the g-factor discussed in the preceding subsection. A quantiative treatment of this contribution has so far not been attempted within the framework of molecular orbital theory. In the present work, we shall also include this type of orbital effect in the case of ^{57m}Fe nucleus and draw conclusions about its importance through comparison between experimental results and our theoretical results.

The spin-contribution to the hyperfine tensor components A_{Nij} for nucleus N can be written in the form [24]:

$$A_{Nij} = A_{NF} + B_{Nij}, \tag{13}$$

where A_{NF} is the isotropic Fermi contact contribution and B_{Nij} refers to the spin dipolar contribution. The former can be further decomposed into [24]:

$$A_{NF} = A_{Nd} + A_{NC} + A_{Np}, \tag{14}$$

where A_{Nd} refers to the direct contribution from the unpaired spin electron:

$$A_{Nd} = a_N \sum_{\mu} |\phi_\mu(0)|^2 \tag{15}$$

and A_{NC} and A_{Np} to the exchange polarization contributions [25a–25e] from the core and paired spin valence electrons. Thus,

$$A_{NC} = a_N \sum_{j(\mathrm{CORE})} [|\chi^{\uparrow}_{jN}(0)|^2 - |\chi^{\downarrow}_{jN}(0)|^2] \tag{16}$$

$$A_{Np} = a_N \sum_{\mu(\mathrm{PAIRED\ MO})} [|\phi^{\uparrow}_{\mu}(0)|^2 - |\phi^{\downarrow}_{\mu}(0)|^2], \tag{17}$$

$$a_N = \frac{8\pi}{6sh} \gamma_e \gamma_N \hbar^2 a_0^{-3} \tag{18}$$

for expressing the A_{Nd}, A_{NC} and A_{Np} in units of Hz. The dipolar tensor component B_{Nij} will in principle also be composed [24] of similar direct and exchange polarization components. However, from atomic calculations [25d, 25e], the

exchange polarization contribution in this case is considered to be relatively small and is usually neglected. Thus B_{Nij}, as given by the direct contribution alone, has the form [24]:

$$B_{Nij} = \frac{3}{8\pi} a_N \sum_{\mu} \left\langle \phi_\mu \left| \frac{3\chi_i\chi_j - r^2\delta_{ij}}{r^5} \right| \phi_\mu \right\rangle. \tag{19}$$

These general expressions for A_{NF} and B_{Nij} have to be treated differently for ^{57m}Fe and ^{14}N nuclei in comparing theory with experiment, because of the difference in the techniques of measurement used in the two cases. Thus, for ^{57m}Fe, the hyperfine interaction tensor has been studied experimentally for both polycrystalline [3b] and single crystal [3c] systems using Mössbauer spectroscopy. For the single crystal system, measurements have been carried out [3c] with the applied magnetic field along the three crystal axes of the monoclinic unit cell of AzidoMb. In order to make comparison with single crystal experimental data, it is necessary to diagonalize the net hyperfine tensor with components A_{Nij} and obtain the principal components and principal axes. However one cannot make direct comparison between theory and experiment for these principal components since the experimental situation is rather complicated, involving four sets of axes, none of which coincide with each other. These four sets are comprised of the heme-based axes in Fig. 1, the crystal axes [3c] *a*, *b* and *c*, the principal axes of the *g*-tensor and the principal axes of the $\boldsymbol{A}_{Fe}$ tensor. Since this type of situation can be quite common for other metal-protein systems including other heme compounds, as well as for many molecular and solid state systems, we have presented in the Appendix a brief derivation of the relationship between the theoretical values of A_{Nij} and the hyperfine splittings they can produce which have to be compared with experiment. The most essential expressions that will be needed for comparison of the theoretical and experimental hyperfine splittings for ^{57m}Fe in AzidoMb, of interest in the present work, will be listed here. Thus, as shown in the Appendix, the effective hyperfine constant that is measured experimentally, for a particular orientation of the applied magnetic field, is given by:

$$A_{eff} = A_{\alpha'\alpha'} l'^2 + A_{\beta'\beta'} m'^2 + A_{\gamma'\gamma'} n'^2, \tag{20}$$

where $A_{\alpha'\alpha'}$, $A_{\beta'\beta'}$ and $A_{\gamma'\gamma'}$ are the principal components of the hyperfine tensor $\boldsymbol{A}$ and l', m' and n' are given by the equations:

$$l' = (\boldsymbol{e}_{eff} \cdot \boldsymbol{e}_{\alpha'}),\ m' = (\boldsymbol{e}_{eff} \cdot \boldsymbol{e}_{\beta'}),\ n' = (\boldsymbol{e}_{eff} \cdot \boldsymbol{e}_{\gamma'}). \tag{21}$$

In Eq. (21), $\boldsymbol{e}_{\alpha'}$, $\boldsymbol{e}_{\beta'}$ and $\boldsymbol{e}_{\gamma'}$ refer to the unit vectors along the principal axes of A, while $\boldsymbol{e}_{eff}$ represents the unit vector along the direction of orientation of the total spin of the molecule in the presence of the applied magnetic field. The orientation of $\boldsymbol{e}_{eff}$ with respect to the principal axes (unit vectors $\boldsymbol{e}_\alpha$, $\boldsymbol{e}_\beta$ and $\boldsymbol{e}_\gamma$) for the *g*-tensor (principal components $g_{\alpha\alpha}$, $g_{\beta\beta}$ and $g_{\gamma\gamma}$) are given by:

$$\boldsymbol{e}_{eff} = \left(\frac{g_{\alpha\alpha} l H_{app}}{H_{eff}}\right) \boldsymbol{e}_\alpha + \left(\frac{g_{\beta\beta} m H_{app}}{H_{eff}}\right) \boldsymbol{e}_\beta + \left(\frac{g_{\gamma\gamma} n H_{app}}{H_{eff}}\right) \boldsymbol{e}_\gamma. \tag{22}$$

H_{app} referring to the magnitude of the applied magnetic field along a direction with direction cosines (l, m, n) with respect to the principal axes of the g-tensor and

$$H_{eff} = \sqrt{g_{\alpha\alpha}^2 l^2 + g_{\beta\beta}^2 m^2 + g_{\gamma\gamma}^2 n^2}\, H_{app}. \tag{23}$$

Thus, for ^{57m}Fe one has to use the appropriate l, m and n for the cases of H_{app} along a, b and c axis in Eq. (23) and then derive A_{eff} to compare with experiment, utilizing Eqs. (20) through (22).

For ^{14}N, the ENDOR spectrum has been observed [2] with the applied magnetic field H_{app} along the direction of the maximum component $g_{\gamma\gamma}$ of the g-tensor, so that $l = m = 0$ and only n has to be considered in Eq. (23).

3. Results and discussion

The results of our calculations will be presented and discussed under a number of categories, namely the energy levels and wave-functions for the d-like states, the spin and charge distributions over the molecule, the g-tensor, the ^{57m}Fe and ^{14}N quadrupole interactions and the magnetic hyperfine interactions of the ^{57m}Fe and ^{14}N nuclei.

3.1. Energy levels and wave-functions for the d-like states

The energy levels of the d-like states, that is, states with predominantly iron d-character, are presented in Fig. 2. In addition to the energy-values for these levels, we have also presented the wave-functions, primarily the d-orbital coefficients. For the sake of brevity, the ligand orbital-admixtures have not been presented explicitly. All the d-like levels, with the exception of the d_{xy}-like, have substantial admixtures of ligand orbitals.

By analogy with the low spin ($S = 1/2$) system ferricytochrome c, whose magnetic and hyperfine properties we have studied earlier [1c], we have assumed that the three lowest d-like states in AzidoMb are populated with five electrons. This leaves the unpaired spin electron in a mixture of d_{xz} and d_{yz} states and leads to

Energy (eV)	Level	Wave-function
−8.1579	———	$0.0000d_{z^2} + 0.0018d_{xz} + 0.8088d_{x^2-y^2} - 0.0005d_{yz} - 0.0000d_{xy} + \sum(\cdots)$
−9.2768	———	$-0.7813d_{z^2} - 0.0244d_{xz} + 0.0000d_{x^2-y^2} - 0.0248d_{yz} - 0.0041d_{xy} + \sum(\cdots)$
−11.1343	———	$-0.0007d_{z^2} + 0.5645d_{xz} - 0.0001d_{x^2-y^2} - 0.5730d_{yz} - 0.0002d_{xy} + \sum(\cdots)$
−11.1454	- - - - - -	$-0.0419d_{z^2} - 0.1366d_{xz} + 0.0001d_{x^2-y^2} - 0.0934d_{yz} - 0.0009d_{xy} + \sum(\cdots)$
−11.2363	———	$-0.0152d_{z^2} - 0.6390d_{xz} + 0.0004d_{x^2-y^2} - 0.6392d_{yz} + 0.0320d_{xy} + \sum(\cdots)$
−11.2639	———	$-0.0009d_{z^2} + 0.0205d_{xz} - 0.0000d_{x^2-y^2} + 0.0204d_{yz} + 0.9832d_{xy} + \sum(\cdots)$
−11.7755	- - - - - - -	$-0.1784d_{z^2} + 0.0929d_{xz} - 0.0003d_{x^2-y^2} + 0.0958d_{yz} + 0.0012d_{xy} + \sum(\cdots)$
−12.4189	- - - - - -	$0.0228d_{z^2} - 0.2137d_{xz} + 0.0019d_{x^2-y^2} - 0.2050d_{yz} - 0.0008d_{xy} + \sum(\cdots)$
−12.6483	- - - - - - -	$-0.0002d_{z^2} + 0.0007d_{xz} + 0.4137d_{x^2-y^2} + 0.0016d_{yz} + 0.0000d_{xy} + \sum(\cdots)$

Fig. 2. d-like (*solid line*) and neighboring ligand-like (*dashed line*) energy levels and wave-functions of AzidoMb. Only the iron $3d$-orbital components of the molecular orbital wave-functions have been shown explictly, the $4s$ and $4p$ and ligand components being included in the summations shown

the strongly rhombic spin distribution suggested by the observed g-tensor [4]. The almost equal admixtures of the d_{xz} and d_{yz} for two of the d-like states actually indicates that they have symmetry close to pure d_{xz} and d_{yz} states but with the X and Y axes pointing in the directions of methine carbons (Fig. 1). The separation between these two levels, which is a reflection of the departure from axial symmetry, was 0.102 eV (823 cm^{-1}), comparing reasonably well with 850 cm^{-1} obtained in earlier work [26] using crystal field analysis. One other feature which we would like to mention is that, because of the significant mixing between iron d-orbitals and ligand orbitals, there are a number of ligand-like states which have substantial iron $3d$-character such as the ones shown by broken lines in Fig. 2. This feature was important for us to consider in the evaluation of the field-gradient tensor at the ^{57m}Fe nucleus and the g-tensor.

3.2. Charge and spin distributions over the system

The charges and unpaired spin populations on the various atoms as obtained by our SCCEH calculations are presented in Table 1. Considering the charge distribution first, one of the major features of the results is that the charges are all quite

Table 1. Charge and unpaired spin populations on atoms[a]

Atom number	Atom type	Charge	Inpaired spin population	Atom number	Atom type	Charge	Unpaired spin population
1	Fe	0.2146	0.6303	26	H	0.0389	0
2	N	−0.1738	0.0027	27	H	0.0249	0
3	N	−0.1740	0.0038	28	H	0.0252	0
4	N	−0.1728	0.0068	29	H	0.0389	0
5	N	−0.1727	0.0055	30	H	0.0255	0
6	C	−0.0062	0.0003	31	H	0.0249	0
7	C	0.0361	0.0051	32	H	0.0395	0
8	C	−0.0252	0.0017	33	H	0.0249	0
9	C	−0.0247	0.0063	34	H	0.0255	0
10	C	0.0355	0.0003	35	H	0.0388	0
11	C	−0.0062	0.0010	36	H	0.0252	0
12	C	0.0355	0.0001	37	H	0.0249	0
13	C	−0.0241	0.0086	38	N	−0.1296	0.0003
14	C	−0.0251	0.0011	39	C	0.0925	0.0003
15	C	0.0371	0.0083	40	N	−0.0209	0
16	C	−0.0052	0.0003	41	C	0.0337	0
17	C	0.0371	0.0079	42	C	0.0170	0.0005
18	C	−0.0252	0.0009	43	H	0.0763	0
19	C	−0.0244	0.0080	44	H	0.2055	0
20	C	0.0355	0.0002	45	H	0.0577	0
21	C	−0.0065	0.00005	46	H	0.0442	0
22	C	0.0355	0.0003	47	N	−0.1770	0.1320
23	C	−0.0248	0.0060	48	N	0.0537	0.0003
24	C	−0.0252	0.0016	49	N	−0.1966	0.1552
25	C	0.0361	0.0048				

[a] The numbers for the atoms correspond to the notations in Fig. 1

small in magnitude. The iron atom carries only a charge of +0.215, substantially smaller than the formal charge of +3 and indicating substantial charge transfer from the Fe^{+3} ion to the other atoms. Similar evidence of strong covalent bonding between iron and its neighbors has been found for other low [1] and high spin [24] heme derivatives. The charge distribution on the porphyrin ring, while being close to tetragonal, does show departures from tetragaonal symmetry due to the presence of the azide and imidazole groups. The nitrogen atoms carry negative charges, with the exception of the central nitrogen atom of the azide group which carries a small positive charge. This suggests that in the localized bond approximation, one can say that the bonding of the azide group with iron and other atoms of the heme group involves an antibonding orbital with a near nodal region at the middle nitrogen atom. The carbon and hydrogen atoms carry relatively small charges, the hydrogen atoms all carrying positive charges while some of the carbon atoms positive and some other negative charges.

Turning next to the spin distribution over the system, the near-tetragonal symmetry is also reflected in the spin distribution. The iron atom carries only 63% of the total unpaired spin population, indicating substantial spin migration to the neighboring atoms as has been found in other high [24, 27] and low [1] spin hemoglobin derivatives. The unpaired spin population transferred from iron appears primarily on the nitrogens of the azide group, the unpaired spin distribution of the latter showing the same feature as the charge distribution, namely, sizeable unpaired spin populations on the two end nitrogens and a small spin population on the central atom. This again suggests that the bonding of the azide group with the heme takes place through an antibonding type orbital with a node close to the central nitrogen atom. The unpaired spin populations on the porphyrin nitrogens are quite small unlike the situation [1c] in ferricytochrome *c* and similar to that [1a] in NOHb. But unlike NOHb, the unpaired spin population on N_ε of the proximal imidazole is rather small, because in contrast to the situation in NOHb where the unpaired spin electron is in a d_{z^2}-like state pointing towards N_ε, the unpaired spin electron in the AzidoMb system is in a state involving a mixture of iron d_{xz} and d_{yz}-like orbitals, for which the Fe–N_ε bond is a nodal line. The reflection of these spin distributions on the hyperfine interactions of the ^{14}N nuclei will be discussed later in this section. In Table 2, we have listed the populations in the *s*, *p* and *d* orbitals of iron, nitrogen and carbon atoms (the *d* orbitals referring to the iron atom) which provide a little more detailed information than Table 1, with the hope that they may be useful for future investigations.

We shall next discuss the *g*-tensor obtained using the calculated electronic wave-functions and energy levels and see how it compares with experiment [4].

3.3. g-Tensor

The components of the *g*-tensor in the co-ordinate system shown in Fig. 1 were evaluated using the perturbation procedure described in Sect. 2.3. and the energy levels and molecular orbital wave-function from our SCCEH investigations,

Table 2. Populations[a] in the *s*, *p* and *d* orbitals of iron, nitrogen and carbon atoms

	s	p_z	p_x	p_y	$3d_{z^2}$	$3d_{xz}$	$3d_{x^2-y^2}$	$3d_{yz}$	$3d_{xy}$
Fe	0.152	0.0854	0.0620	0.0644	0.4180	0.9599	0.4741	0.9675	0.9982
	0.152	0.0854	0.0620	0.0644	0.4180	0.6495	0.4741	0.6475	0.9982
N_2	0.6804	0.6860	0.6585	0.5634					
	0.6804	0.6845	0.6573	0.5634					
N_3	0.6803	0.6855	0.5633	0.6565					
	0.6803	0.6831	0.5633	0.6551					
N_4	0.6807	0.6880	0.6599	0.5634					
	0.6807	0.6826	0.6585	0.5634					
N_5	0.6776	0.6883	0.5637	0.6586					
	0.6776	0.6841	0.5637	0.6573					
C_6	0.5493	0.4912	0.4818	0.4823					
	0.5493	0.4910	0.4818	0.4822					
C_7	0.5572	0.5314	0.4644	0.4311					
	0.5572	0.5264	0.4644	0.4311					
C_8	0.5529	0.5091	0.4668	0.4847					
	0.5529	0.5075	0.4667	0.4847					
C_9	0.5530	0.5236	0.4670	0.4849					
	0.5530	0.5173	0.4670	0.4849					
C_{10}	0.5571	0.5301	0.4639	0.4308					
	0.5571	0.5299	0.4639	0.4307					
C_{11}	0.5494	0.4915	0.4822	0.4818					
	0.5494	0.4905	0.4822	0.4818					
C_{12}	0.5571	0.5309	0.4307	0.4639					
	0.5571	0.5309	0.4307	0.4638					
C_{13}	0.5532	0.5106	0.4853	0.4670					
	0.5532	0.5020	0.4853	0.4670					
C_{14}	0.5527	0.5090	0.4848	0.4698					
	0.5527	0.5081	0.4847	0.4697					
C_{15}	0.5572	0.5321	0.4312	0.4648					
	0.5572	0.5239	0.4312	0.4647					
C_{16}	0.5489	0.4905	0.4813	0.4816					
	0.5489	0.4903	0.4812	0.4815					
C_{17}	0.5573	0.5316	0.4646	0.4311					
	0.5573	0.5238	0.4645	0.4311					
C_{18}	0.5527	0.5088	0.4665	0.4849					
	0.5527	0.5081	0.4664	0.4848					
C_{19}	0.5497	0.5101	0.4674	0.4850					
	0.5497	0.5021	0.4674	0.4850					
C_{20}	0.5570	0.5303	0.4638	0.4307					
	0.5570	0.5303	0.4637	0.4306					
C_{21}	0.5493	0.4908	0.4817	0.4816					

Table 2 (continued)

	s	p_z	p_x	p_y	$3d_{z^2}$	$3d_{xz}$	$3d_{x^2-y^2}$	$3d_{yz}$	$3d_{xy}$
C_{22}	0.5571	0.5306	0.4304	0.4637					
	0.5571	0.5304	0.4304	0.4636					
C_{23}	0.5529	0.5096	0.4851	0.4669					
	0.5529	0.5036	0.4851	0.4669					
C_{24}	0.5528	0.5090	0.4847	0.4666					
	0.5528	0.5075	0.4847	0.4665					
C_{25}	0.5574	0.5313	0.4310	0.4642					
	0.5574	0.5265	0.4310	0.4642					
N_{38}	0.6704	0.6952	0.5817	0.6182					
	0.6704	0.6951	0.5816	0.6181					
C_{39}	0.5505	0.4121	0.4722	0.5184					
	0.5505	0.4120	0.4721	0.5183					
N_{40}	0.6287	0.5717	0.6139	0.6958					
	0.6287	0.5717	0.6139	0.6958					
C_{41}	0.5477	0.4865	0.4357	0.5130					
	0.5477	0.4865	0.4357	0.5130					
C_{42}	0.5532	0.4637	0.4542	0.5198					
	0.5532	0.4635	0.4541	0.5197					
N_{47}	0.7108	0.5930	0.6802	0.6816					
	0.7108	0.5929	0.6153	0.6146					
N_{48}	0.6285	0.6536	0.5945	0.5944					
	0.6285	0.6536	0.5943	0.5943					
N_{49}	0.7304	0.6019	0.6764	0.6781					
	0.7304	0.6019	0.6003	0.5990					

[a] The upper and lower sets of numbers refer to the populations in the atomic like states with spin parallel and antiparallel to the spin of the unpaired molecular orbital state. The suffices for the atoms correspond to the atom numbers in Table 1 and Fig. 1

whose features are described earlier in this section. The g-tensor obtained in this manner is non-diagonal and is given by:

$$g = \begin{pmatrix} 2.69 & -0.06 & -0.06 \\ -0.06 & 2.24 & 0.30 \\ -0.06 & 0.30 & 2.25 \end{pmatrix} \tag{24}$$

the order of the axes being Z, X and Y. While the major contributions to the departure from free-electron value for the diagonal components arises from excitations between d-like levels (for g_{zz} from excitations from the lower doubly occupied d_{xz}-d_{yz} like level in Fig. 2 to the unpaired spin level and for g_{xx} and g_{yy} from corresponding excitations for the d_{xy}-like level), there are also significant contributions from other levels which can be characterized as ligand-like levels. One of these is the level indicated by a broken line in Fig. 2 lying in between the two t-type states which have mixtures of d_{xz} and d_{yz} characters.

On diagonalization of the g-tensor in Eq. (19), we get the principal components

$$g_{z'z'} = 2.73, \qquad g_{y'y'} = 2.51, \qquad g_{x'x'} = 1.95, \tag{25}$$

with the direction cosines of the principal axes z', x' and y' with respect to the laboratory axes in Fig. 1 being given by

$$V_{ii'} = \begin{pmatrix} 0.92 & 0.00 & 0.40 \\ -0.28 & 0.71 & 0.64 \\ -0.29 & -0.70 & 0.65 \end{pmatrix}, \tag{26}$$

where the order of the columns i is z', x' and y' and that of the rows i is z, x and y. The principal axis corresponding to the largest component is oriented at an angle of 23° with respect to the heme normal, the axis corresponding to the smallest principal component lying on the XY plane and oriented at an angle of 44° with respect to the X-direction (Fig. 1). The g-tensor has been studied experimentally by three different groups [4]. One of the measurements has been carried out [4a] in a polycrystalline sample and the other two [4b, 4c] in single crystal systems. For the single crystal measurements [4b, 4c], the orientations of the principal axes have been given with respect to the crystal axes of the monoclinic lattice. The direction of the maximum principal component from our investigation is seen to depart from the heme normal, a feature in agreement with a similar conclusion from the single crystal measurements [4b, 4c]. The angle of inclination of 23° with respect to the heme normal obtained from our work is larger than the angle of about [4d] 9° from single crystal measurements. Both the single crystal measurements [4b, 4c] however indicate that the x' axis, representing the direction for the smallest principal component of the g-tensor, lies on the heme plane, in agreement with our results. Additionally, the x' direction, from our theoretical investigations, makes an angle of 44° to the line joining Fe to one of the porphyrin nitrogens, its orientation being in the middle of those obtained from the two single crystal measurements [4b, 4c].

As regards the experimental magnitudes of the principal components of the g-tensor, the polycrystalline measurement leads to the values [4a] (2.81, 2.19, 1.61), in close agreement with the values (2.82, 2.19, 1.72) [4b] and (2.80, 2.22, 1.72) [4c] from single crystal measurements. From Eq. (20), it can be seen that the agreement between theory and experiment is quite satisfactory, especially for the largest component. The latter features, using Eq. (7), suggests that the wave-functions for the two states involving mixtures of d_{xz} and d_{yz} characters and their separations are quite accurate, since it is the excitation process involving these states that produces the major departure of g_{zz} from free electron character and $g_{z'z'}$ from Eqs. (24) and (25) is seen to be quite close to g_{zz} in magnitude. The principal components $g_{x'x'}$ and $g_{y'y'}$ in Eq. (25) are somewhat larger than experiment, suggesting that the separation between the d_{xy}-like level and the unpaired spin level should be somewhat smaller than is obtained by the SCCEH procedure. It would be interesting to test this point by first-principle self-consistent Hartree–Fock calculations [28] as well as the approximation to the Hartree–Fock method referred to as the multiple scattering-X_α procedure

[29]. Additionally as discussed elsewhere, one should also examine possible contributions from other mechanisms, one of them being the exchange polarization mechanism [30] involving differences between the energies and wavefunctions for up and down spin states of the doubly occupied molecular orbitals, which results from the exchange interaction of the unpaired spin electrons with the occupied up spin states. A second mechanism that should be examined is the Casimir mechanism [31], which gives an additional contribution in relativistic theory besides that arising from the spin-orbit mechanism discussed in Sect. 2.3.

The most important point about the results of our theoretical analysis is that it shows that one can explain the observed rhombic nature [4] of the g-tensor with the choice of the electronic structure for the molecule as one involving five electrons in d-like states, the unpaired spin electron being in a t-state (the corresponding molecular orbital involving a mixture of d_{xz} and d_{yz}-type symmetry), as was also expected from crystal field theory [26]. We shall use this electronic structure to analyze available ^{57m}Fe nuclear quadrupole interaction and magnetic hyperfine data from Mössbauer measurements [3] and ^{14}N nuclear quadrupole and magnetic hyperfine interaction data from ENDOR experiments [2]. If one had assumed an electronic configuration with seven d-like electrons, as in nitrosylhemoglobin [1a], with the unapired spin electron in an e-type state such as a d_{z^2}-like or $d_{x^2-y^2}$-like molecular orbital, the g-tensors one obtains, using the procedure in Sect 2.3, have components (2.124, 2.033, 2.034) and (2.00, 2.160, 2.161) respectively, which are almost axially symmetric and close to free electron like, in distinct disagreement with experiment [4].

3.4. ^{57m}Fe *nuclear quadrupole interaction*

We shall next discuss the application of the calculated electronic structure with five d-like electrons in t-type states, which has been successful in explaining g-tensor data, to understand available ^{57m}Fe quadrupole interaction data from Mössbauer measurements [3]. The quadrupole splitting has been measured both in powdered samples [3a] as well as in the single crystal [3b, 3c]. The two polycrystalline measurements have yielded very similar quadrupole splittings, the more recent value [3b] being 2.25 mm/s. The single crystal measurement [3c] has provided values for the coupling constant e^2qQ and asymmetry parameter η of (-2.1 ± 0.05) mm/s and (0.4 ± 0.1) respectively.

In our investigation, we have obtained the components of the field-gradient tensor in the coordinate system shown in Fig. 1 and then diagonalized it, as in the case of the g-tensor. From the principal components, we have obtained the quadrupole splittings using Eq. (11) with the standard convention for q and η (see Eq. (10)), as discussed in Sect. 2.4. For the quadrupole moment Q (^{57m}Fe) to be used in Eq. (10), the recent value [15] of 0.082 barns has been utilized. This value was derived through the analysis of Mössbauer nuclear quadrupole interaction data [32] in $FeCl_2$ and $FeBr_2$ molecules using electric field-gradients obtained from first-principles Hartree–Fock investigations [15a] of the electronic structures in these molecules. This value of $Q(^{57m}\text{Fe})$, which is less than one half of that in use prior to the work in [15a] has been supported by subsequent analyses of

nuclear quadrupole interaction data in ionic crystals [15b] and metallic alloys [15c].

In calculating the electric field gradient tensor components using Eq. (12), all paired and unpaired spin orbitals ϕ_μ have been utilized. Since the effective charges on the ligand atoms are quite small, contributions from the nuclear charges and atomic orbital components of the molecular orbitals associated with the ligand atoms have been neglected, assuming these contributions to cancel, as in earlier work [24c], and only the contributions from the $3d$, $4s$ and $4p$ orbital components associated with the iron atom have been retained.

By this procedure, the field gradient tensor components obtained in the coordinate axis system shown in Fig. 1, are given by:

$$\boldsymbol{V} = \begin{pmatrix} 1.19 & 0.02 & 0.01 \\ 0.02 & -0.60 & -1.21 \\ 0.01 & -1.21 & -0.59 \end{pmatrix}, \tag{27}$$

with the choice of the rows and columns in the order Z, X and Y. In Eq. (27), the components of $\boldsymbol{V}$ are stated in mm/s. They actually refer to the components V_{ij} multiplied by $\frac{1}{2}e^2qQ$, because this factor occurs in the expression in Eq. (11) for the quadrupole splitting. To obtain the field-gradient components in units of ea_0^{-3} from the components in Eq. (27), one has to divide the latter by a factor of 0.8301, using the recent value [15] for $Q(^{57m}\mathrm{Fe})$.

On diagonalization, the tensor in Eq. (27) leads to the principal components

$$V_{z'z'} = -1.81, \qquad V_{x'x'} = 0.61 \quad \text{and} \quad V_{y'y'} = 1.195, \tag{28}$$

with direction cosines V_{ii}, describing the orientations of the principal axes z', x' and y' in Fig. 1, given by:

$$V_{ii'} = \begin{pmatrix} 0.01 & 0.00 & 1.00 \\ -0.71 & -0.71 & 0.00 \\ -0.71 & 0.71 & 0.00 \end{pmatrix}. \tag{29}$$

The orders of the columns and rows are chosen in the same way as in Eq. (27), the columns representing in order the direction cosines for the principal axes z', x' and y'.

From the principal components of $\boldsymbol{V}$ in Eq. (28), the asymmetry parameter, using Eq. (10) is given by

$$\eta = 0.32 \tag{30}$$

Thus the field-gradient tensor, like the g-shift tensor, is predicted to be substantially rhombic in character. But the two tensors are rather different in nature, the quadrupole coupling tensor having its largest component lying on the XY-plane and making an angle close to 45° with respect to the X-axis. The largest component of $\boldsymbol{g}$ obtained from theory, as discussed earlier, is oriented in a direction inclined at about 23° to the heme normal.

In comparing with experiment, our theoretical value of the quadrupole splitting, using Eq. (11) and the principal components of $\boldsymbol{V}$ in Eq. (28), comes out as 1.83 mm/s in satisfactory agreement with the experimentally observed splitting of 2.25 mm/s from Mössbauer measurement [3b] on polycrystalline samples. The calculated values of the principal component $V_{z'z'}$ in Eq. (28) and η in Eq. (30) are also in satisfactory agreement with the corresponding measured values [3c] of (-2.10 ± 0.05) mm/s and (0.4 ± 0.1) in the single crystal. Further, the z' axis corresponding to the largest principal component of $\boldsymbol{V}$ is found to lie on the porphyrin plane from both theory (Eq. (29)) and single crystal measurements [3c]. The angle between z' and the X-axis (one of the Fe-N directions) was found from the present work to be about 44°, somewhat larger than the single crystal value [3c] of 32°. However, interestingly, the z'-axis for the field gradient tensor is found to be nearly perpendicular to the x'-axis for the $\boldsymbol{g}$-tensor (corresponding to the smallest principal component $g_{X'X'}$ from both the work here and single crystal [3c] Mössbauer data.

3.5. *^{14}N quadrupole interaction*

The ^{14}N nuclear quadrupole interaction, like ^{57m}Fe, derives contributions from both the paired and unpaired spin orbitals and will be derived using the same local approximation to Eq. (12) as for ^{57m}Fe. This approximation is even more satisfactory here due to the smaller antishielding factor, which further reduces the importance of contributions to the field-gradient from other atoms. For the ENDOR technique used to study the ^{14}N quadrupole interaction, the pertinent experimental quantity is P_{zz} which is $\frac{3}{4} e^2qQ$, where q is the field gradient at the ^{14}N site along the direction in which the magnetic field is applied. The values of P_{zz} in MHz in Table 3 correspond to the Z-axis taken along the heme normal.

Experimental data [2] on P_{zz} for ^{14}N nuclei are presently available only for the porphyrin nitrogens. The association of the observed ENDOR signals with the porphyrin nitrogens has been made [2] through a selective substituion procedure involving replacement of ^{14}N nuclei by ^{15}N. Two sets of ENDOR patterns have been observed [2], leading to $P_{zz} = 0.62$ MHz and 0.55 MHz. These data are in satisfactory agreement with our theoretical results for the four porphyrin nitrogens in Table 3. It should be remarked however that the Z-axis for P_{zz} from the experimental data [2] corresponds to the direction of the maximum component

Table 3. ^{14}N magnetic and nuclear quadrupole hyperfine constants[a] (MHz)

	N_1	N_2	N_3	N_4	N_ε	N_δ	N_α	N_β	N_γ
A_F	0.160	0.141	0.141	0.169	0.007	0.003	0.008	0.000	0.000
B_{zz}	0.126	0.253	0.676	0.506	−0.010	0.000	−9.303	−0.034	−10.556
A_{zz}	0.286	0.394	0.817	0.675	−0.003	0.000	−9.302	−0.034	−10.556
P_{zz}	0.645	0.641	0.624	0.638	0.825	−0.727	−0.296	0.816	−0.434

[a] Z-direction used here corresponds to heme normal. The atoms N_1, N_2, N_3 and N_4 correspond to the porphyrin nitrogens N_2 through N_5 in Fig. 1 and Table 2, N_ε and N_δ refer to the imidazole nitrogens N_{38} and N_{40} while N_α, N_β and N_γ correspond to the three azide nitrogens

of the g-tensor. Since, as discussed already in Sect 3.3, this direction has been found experimentally [4b] to be inclined at about 9° to the heme normal, one would not expect any significant difference between the theoretical results in Table 3 and those corresponding to the Z-direction for the experimental data.

Thus our results for the g-tensor and ^{57m}Fe and ^{14}N quadrupole interactions are in satisfactory agreement with experiment. This provides support for the electronic structure from our SCCEH investigations based on the assumption that five electrons are present in the t-type d-like molecular orbital states. This assignment had also been suggested by earlier crystal field analysis [4a, 3a] of the g-tensor and ^{57m}Fe quadrupole interaction data. We shall next examine the results that one expects for the ^{57m}Fe and ^{14}N magnetic hyperfine interactions using our calculated electronic wave functions and make comparisons with the corresponding data from Mössbauer [3c] and ENDOR [2] measurements.

3.6. ^{57m}Fe *magnetic hyperfine interaction*

In analyzing the magnetic hyperfine interactions, we shall first consider the case of ^{57m}Fe. The hyperfine interaction associated with ^{14}N nuclei will be discussed in Sect. 3.7.

As discussed in Sect 2.4., the hyperfine interaction tensor is composed of contributions from contact and dipolar effects as in Eq. (14). In evaluating the contact contribution, one has, as in Eq. (14), to consider [24] the effects of direct contribution from the unpaired electrons and the exchange polarization contribution from the paired spin core and valence electrons. The direct contributions A_d can be obtained from Eq. (15) using the calculated wave function for the unpaired spin electron. However for the exchange polarization contributions from the core and valence electrons, we cannot use Eqs. (16) and (17) directly, because we have not performed an unrestricted Hartree-Fock calculation [20] with different wave functions for paired states of opposite spins. We shall therefore use the approximations to the Eqs. (16) and (17) that have been employed previously [24] to successfully explain the ^{57m}Fe hyperfine constants for high spin heme compounds. These approximations are represented by the following equations [24a]:

$$A_{\mathrm{Fe,c}} = \frac{q'_{3d,u}}{q_{3d,u}} a_{\mathrm{Fe}} \sum_{j=1} (|\chi^{\uparrow}_{\mathrm{Fe}js}(0)|^2 - |\chi^{\downarrow}_{\mathrm{Fe}js}(0)|^2) \tag{31}$$

$$A_{\mathrm{Fe,p}} = \frac{q'_{3d,u} q'_{4s,p}}{q_{3d,u} q_{4s,p}} a_{\mathrm{Fe}} (|\chi^{\uparrow}_{\mathrm{Fe}4s}(0)|^2 - |\chi^{\downarrow}_{\mathrm{Fe}4s}(0)|^2), \tag{32}$$

where $q'_{3d,u}$ represents the net unpaired spin population in iron $3d$ states in AzidoMb obtained from the present calculation using the Mulliken approximation and $q_{3d,u} = 4$ is the $3d$ unpaired spin population in neutral iron atom in the ground state, ^5S. The quantity $q'_{4s,p}$ refers to the paired spin population in the $4s$ states in the molecule again using the Mulliken approximation and $q_{4s,p} = 2$ is the $4s$ population in the neutral iron atom. The $\chi^{\uparrow}_{\mathrm{Fe}js}$ and $\chi^{\downarrow}_{\mathrm{Fe}js}$ $(j = 1-4)$, represent the spin polarized s orbital wave functions and a_{Fe} is obtained from Eq. (18) using

the magnetogyric ratio γ_{Fe} for γ_N. Eqs. (31) and (32) are obtained by essentially weighting [24a] the exchange polarization contribution from the core s and $4s$ states in free iron atom by the ratios of the unpaired spin and $4s$ paired spin populations in the molecule and the free atom.

For the dipolar hyperfine tensor, Eq. (19) was used to obtain the components in the molecule based system with Z-axis perpendicular to the heme plane and X and Y-axes as shown in Fig. 1. The contributions to B_{Nij} could arise from orbitals on iron as well as those on the ligands. Contributions from the latter were found to be negligible as in the case of the ^{57m}Fe nuclear quadrupole interaction. Thus, only the local contributions involving the iron orbital components of the unpaired spin molecular orbitals had to be included. In principle, while these components would include the iron $3d$, $4s$ and $4p$ orbital components in the unpaired spin molecular orbitals, only $3d$ orbitals were needed to be considered for B_{Nij}, because of their dominant amplitudes, leading to

$$B_{Feij} = \frac{3}{8\pi} a_{Fe} \sum_{\mu kl} C_{\mu d_k} C_{\mu d_l} \left\langle \chi_{3d_k} \left| \frac{3\chi_i\chi_j - r^2\delta_{ij}}{r^5} \right| \chi_{3d_l} \right\rangle, \tag{33}$$

where k and l refer to the five d orbitals with z^2, x^2-y^2, xy, xz and yz symmetry. As remarked in Sect. 2.4., the exchange core polarization effect is usually assumed [24] to be small for the dipolar contribution and has not been included.

We have used Eqs. (15), (31), (32) and (33) to obtain the contact, dipolar and total fields at the ^{57m}Fe nucleus as shown in Eqs. (34)–(37). To express the hyperfine interaction tensor in terms of the hyperfine field components at the nucleus in units of kiloGauss (kG), the expression that has to be used for the factor a_{Fe} is $(8/3)\pi\mu_B a_0^{-3}$ with a numerical value of 524.2 kG. The principal components of the dipolar field tensor $\boldsymbol{B}$ are obtained as usual by diagonalizing the tensor with components B_{Nij} given by Eq. (33). By these procedures, for the contact isotropic hyperfine field, the direct, exchange polarization contributions from both core and valence electrons and the sum total of the three, are obtained as:

$$A_{Fe,d} = 0.00$$

$$A_{Fe,c} = -82.19$$

$$A_{Fe,p} = 10.12$$

$$A_{Fe,total} = -72.06.$$

The principal components of the dipolar field are given by:

$$B_{z'z'} = -118.58$$

$$B_{x'x'} = 59.32 \tag{35}$$

$$B_{y'y'} = 59.26$$

the orientation of the principal axes being described by the direction cosines in Eq. (36) with respect to the molecule based axes system.

$$\gamma_{ii'} = \begin{pmatrix} 0.00 & 0.71 & 0.71 \\ 0.70 & -0.50 & 0.50 \\ 0.71 & 0.50 & -0.50 \end{pmatrix}, \tag{36}$$

where, as in the case of the g-tensor, the order of the columns i' is z', x' and y' while that of the rows i is z, x and y. On combining Eqs. (34) and (35), the principal components of the total hyperfine field are given by Eq. (37)

$$\begin{aligned} A_{z'z'} &= -190.64 \\ A_{x'x'} &= -120.80 \\ A_{y'y'} &= -12.74 \end{aligned} \tag{37}$$

the principal axes for the total hyperfine field being the same as for the dipolar.

As pointed out in Sect. 2.4. the hyperfine fields at the ^{57m}Fe nucleus in the single crystal have been measured [3c] with the applied magnetic field in the direction of the crystallographic axes corresponding to the monoclinic unit cell. One has therefore to make use of Eqs. (20)-(23) together with the principal axes for the $\boldsymbol{A}$ and $\boldsymbol{g}$ tensors obtained from our calculations. The quantities $A_{\alpha'\alpha'}$, $A_{\beta'\beta'}$ and $A_{\gamma'\gamma'}$ in Eq. (20) correspond to $A_{z'z'}$, $A_{x'x'}$ and $A_{y'y'}$ in Eq. (37). For the quantities l', m', n' in Eq. (20), Eq. (21) indicates one needs a knowledge of the unit vectors $\boldsymbol{e}_{\text{eff}}$ and $\boldsymbol{e}_{\alpha'}$, $\boldsymbol{e}_{\beta'}$, $\boldsymbol{e}_{\gamma'}$. The latter three vectors, using the direction cosines in Eq. (36), are given by

$$\begin{aligned} \boldsymbol{e}_{\alpha'} &= 0.71\boldsymbol{i} + 0.71\boldsymbol{j} + 0.00\boldsymbol{k} \\ \boldsymbol{e}_{\beta'} &= -0.50\boldsymbol{i} + 0.50\boldsymbol{j} + 0.71\boldsymbol{k} \\ \boldsymbol{e}_{\gamma'} &= 0.50\boldsymbol{i} - 0.50\boldsymbol{j} + 0.71\boldsymbol{k}, \end{aligned} \tag{38}$$

where $\boldsymbol{i}$, $\boldsymbol{j}$ and $\boldsymbol{k}$ correspond to the unit vectors in the molecule based coordinate system For the vector $\boldsymbol{e}_{\text{eff}}$, one has to use Eq. (22) which requires a knowledge of the principal components of $\boldsymbol{g}$ given by Eq. (25), the orientations of the principal axes of $\boldsymbol{g}$ obtainable from the direction cosines in Eq. (26), $H_{\text{app}}/H_{\text{eff}}$ given by Eq. (23) and the direction cosines (l, m, n) for each of the crystal axes, a, b and c with respect to the principal axes of the $\boldsymbol{g}$-tensor. Thus $\boldsymbol{e}_\alpha$, $\boldsymbol{e}_\beta$ and $\boldsymbol{e}_\gamma$ in Eq. (22) are given by:

$$\begin{aligned} \boldsymbol{e}_\alpha &= 0.71\boldsymbol{i} - 0.70\boldsymbol{j} + 0.00\boldsymbol{k} \\ \boldsymbol{e}_\beta &= 0.64\boldsymbol{i} + 0.65\boldsymbol{j} + 0.40\boldsymbol{k} \\ \boldsymbol{e}_\gamma &= -0.28\boldsymbol{i} - 0.29\boldsymbol{j} + 0.92\boldsymbol{k}. \end{aligned} \tag{39}$$

The unit vectors corresponding to a, b and c axes, using crystal structure data

[3c, 6], are given by:

$$\begin{aligned} \boldsymbol{e}_a &= -0.07\boldsymbol{i} - 0.44\boldsymbol{j} + 0.89\boldsymbol{k} \\ \boldsymbol{e}_b &= 0.66\boldsymbol{i} + 0.66\boldsymbol{j} + 0.37\boldsymbol{k} \\ \boldsymbol{e}_c &= -0.71\boldsymbol{i} + 0.71\boldsymbol{j} + 0.00\boldsymbol{k}. \end{aligned} \tag{40}$$

The direction cosines l, m and n in Eq. (22) for the a-axis are given by the scalar products of $\boldsymbol{e}_a$ with $\boldsymbol{e}_\alpha$, $\boldsymbol{e}_\beta$ and $\boldsymbol{e}_\gamma$ respectively. The corresponding direction cosines for the b and c crystal axes can be obtained by taking the scalar products of $\boldsymbol{e}_b$ and $\boldsymbol{e}_c$ respectively with $\boldsymbol{e}_\alpha$, $\boldsymbol{e}_\beta$ and $\boldsymbol{e}_\gamma$.

Using Eq. (23), together with Eqs. (25) and (40), one obtains

$$\frac{H_{\text{eff}}}{H_{\text{app}}} = 2.688, 2.542 \quad \text{and} \quad 1.948 \tag{41}$$

for the magnetic field applied along the a, b and c axes. Next, using Eqs. (22), (25), (39) and (40), the unit vectors $\boldsymbol{e}_{\text{eff}}$ for applied magnetic fields along the a, b and c axes are given by

$$\begin{aligned} \boldsymbol{e}_{\text{eff}}(a) &= -0.12\boldsymbol{i} - 0.40\boldsymbol{j} + 0.91\boldsymbol{k} \\ \boldsymbol{e}_{\text{eff}}(b) &= 0.65\boldsymbol{i} + 0.66\boldsymbol{j} + 0.37\boldsymbol{k} \\ \boldsymbol{e}_{\text{eff}}(c) &= -0.71\boldsymbol{i} + 0.71\boldsymbol{j} - 0.00\boldsymbol{k} \end{aligned} \tag{42}$$

Finally, using Eqs. (20), (21) and (42), the value of the effective hyperfine fields for applied magnetic fields along a, b and c axes are given by:

$$A_{\text{eff}}(a) = -37.03, \qquad A_{\text{eff}}(b) = -165.95, \qquad A_{\text{eff}}(c) = -12.79 \quad \text{(kG)} \tag{43}$$

The theoretical results in Eq. (43) have to be compared with the corresponding experimental results [3c] obtained from Mössbauer measurements, namely $|184 \pm 5|$, $|133 \pm 5|$ and $|99 \pm 5|$ kiloGauss respectively. There is good order of magnitude agreement with experiment and also reasonable numerical agreement for $A_{\text{eff}}(b)$. However, the magnitudes of $A_{\text{eff}}(a)$ and $A_{\text{eff}}(c)$ appear to be significantly underestimated. Part of the problem could be the inaccuracy of the electronic wave functions and one should in future test the results in Eq. (43) by using wave functions obtained by other methods. However, the reasonable agreements between theory and experiment for the quadrupole interactions of ^{57m}Fe and ^{14}N nuclei suggest that the calculated electron distributions are quite reliable. Possible improvements in the value of the isotropic hyperfine field A_{F} by the use of a less empirical procedure for determining the core-polarization and paired valence electron polarization than that used here [24] could also influence the theoretically obtained magnitudes of the $A_{\text{eff}}(a)$, $A_{\text{eff}}(b)$ and $A_{\text{eff}}(c)$. However, the fact that there is a difference in the trends in the magnitudes of these fields between theory and experiment suggests that the tensor components $B_{z'z'}$, $B_{x'x'}$, and $B_{y'y'}$ and the orientations of the principal axes z', x' and y' are more likely responsible for the underestimation of $A_{\text{eff}}(a)$ and $A_{\text{eff}}(c)$ than the isotropic contribution. It appears that the most likely source [33] for changes in the tensor contribution to the hyperfine field is the influence of the orbital effect that can arise from the

unquenching of the orbital angular momentum through the spin-orbit interaction associated with the iron atom, discussed in Sect. 2.3. This unquenching effect is of course responsible for the departure of the g-tensor from feee spin character. We have recently carried out a variational calculation for the influence of spin-orbit interaction on the electronic wave function for the AzidoMb system and evaluated the dipolar and orbital contributions to the hyperfine tensor for ^{57m}Fe nucleus. The latter of course vanishes when spin-orbit effects are not included. The procedure is too involved to describe here but will be presented as a separate communication [34]. The principal components of the hyperfine tensor obtained after combining the isotropic contact, orbital and dipolar contributions to the hyperfine field, are found to be

$$A_{x'x'} = 45.33, \qquad A_{y'y'} = 119.61 \quad \text{and} \quad A_{z'z'} = 275.06 \quad \text{(kG)} \tag{44}$$

differing very substantially from the results in Eq. (37), The y-matrix for the orientations of the principal axes x', y' and z' is given by,

$$y_{ii'} = \begin{pmatrix} -0.86 & -0.51 & 0.04 \\ -0.51 & 0.86 & 0.02 \\ 0.05 & 0.00 & 0.99 \end{pmatrix}, \tag{45}$$

which replaces Eq. (36) obtained without including spin-orbit interaction effects. Following the procedure discussed earlier in this section and involving Eqs. (38)-(42), the hyperfine fields for applied magnetic fields along a, b and c axes are given by:

$$A_{\text{eff}}(a) = 252.36, \qquad A_{\text{eff}}(b) = 133.36, \qquad A_{\text{eff}}(c) = 116.20 \quad \text{(kG)} \tag{46}$$

differing very substantially from the values in Eq. (43) and in fairly satisfactory agreement with experimental results. These results suggests that spin-orbit effects [33] must be included in the study of ^{57m}Fe hyperfine fields for low spin hemoglobin derivatives.

3.7. ^{14}N *magnetic hyperfine interaction*

As in the case of ^{57m}Fe hyperfine interaction just discussed, for ^{14}N nucleus also, one can have contributions [24, 33] from contact, dipolar and orbital mechanisms. The orbital mechanism [33], however, is expected to be rather weak because of the relatively small spin orbit interaction associated with the nitrogen atom. For the constact and dipolar mechanisms [24], one can have both direct and exchange polarization contributions. Since the procedure used here for obtaining the wave functions is a spin-restricted one, one cannot make direct use of Eqs. like (16) and (17) and has to devise other ways to include these effects. In the case of iron, the major part of the unpaired spin population (63%) is located on the iron atom itself, as can be seen from Table 1, but in the case of the nitrogen atoms, there are only small amounts of unpaired spin populations on these atoms. Therefore, unlike the case of iron, the exchange polarization effect is expected to be less pronounced and arise from both the unpaired spin population on the nitrogen in question as well as those on neighboring atoms. These latter contributions are difficult to calculate. We shall therefore compare the direct contributions with experiment and try to examine in this way the relative importance of the

exchange polarization contribution. A part of the latter contribution can be obtained through the use of semi-empirical formulae available in the literature [35] and will also be discussed.

In Table 3, the contact and dipolar contributions are presented for all the nitrogens associated with the heme unit and its imidazole and azide ligands. Since the ENDOR measurements [2] are carried out with the magnetic field along the direction of the maximum principal component of the g-tensor, one needs, as in the case of the quadrupole interaction discussed earlier (Sect. 3.5), the components A_{zz} of the hyperfine tensors along the same direction for the various nitrogen atoms to make comparisons with the experimental results. In Table 3, we have presented the results for the case where the Z-direction is along the heme normal. Since, the direction for the largest principal component is only 9° from the heme normal, one again does not expect any significant difference between the results for the two directions.

From Table 3, the contact contributions are all seen to be quite small for the porphyrin nitrogens and nearly negligible for the imidazole nitrogens and the central azide nitrogen N_β, but rather large negative for the other two nitrogens N_α and N_γ of the azide group, (N_α being the atom bonded to iron). The latter feature is most likely a consequence of the fact that the unpaired electron orbital which involves mixtures of d_{xz} and d_{yz} symmetry about the iron atom, conjugates strongly with π-orbitals on the azide group. The net hyperfine constants A_{zz} appear to be all less than 1 MHz for porphyrin nitrogens, negligible for the imidazole nitrogens and close to -10 MHz for the azide nitrogens N_α and N_γ.

For comparison with experiment, one notes that the ENDOR hyperfine data [2] from ^{15}N substitution measurements indicate that the observed A_{zz} refer to porphyrin nitrogens, there being two sets of experimental ^{14}N hyperfine constants, namely 5.64 and 6.14 MHz. Ascribing these to the N_3 and N_4 porphyrin nitrogens, which are seen from our theoretical results in Table 3 to be the largest among the four porphyrin nitrogens, the theoretical values of A_{zz} appear to be about a factor of 6 smaller than experiment [2].

In looking for sources that could remove the difference between the theory and experiment, one is first tempted to ascribe the observed hyperfine constants to N_α and N_γ at the azide group, but the ^{15}N substitution measurement [2] rules this out. Another possibility is that the unpaired spin electron is in a state of $d_{x^2y^2}$ or d_{z^2} symmetry with seven d-type electrons present as in the case of nitrosylmyoglobin [1a]. These would lead to hyperfine constants A_{zz} of 2.12, 2.22, 2.21 and 2.12 MHz for the porphyrin nitrogens N_1, N_2, N_3 and N_4 respectively for the d_{z^2}-like unpaired orbital case and 10.84, 10.95, 10.86 and 10.78 MHz for the d_{x^2}-y^2 case, both these sets of values being closer to experiment than the results in Table 3. But as discussed in Sect. 3.3, the choice of either of these configurations leads to an axially symmetric g-tensor with the components close to free-electron like, both features in complete disagreement with the observed [3] strongly rhombic g-tensor for the molecule. These configurations can also be

ruled out from a consideration of ^{57m}Fe nuclear quadrupole interaction parameters $1/2\ e^2qQ$ and asymmetry parameter η. Thus, for the configurations with d_{z^2} and $d_{x^2-y^2}$ in unpaired spin orbital states, the values of $1/2\ e^2qQ$ are given by -0.8 mm/s and -2.85 mm/s respectively and $\eta = 0$ in sharp disagreement with results of Mössbauer measurements [3b, 3c]. Our analyses in Sect. 3.3 and 3.4 of the g and quadrupole interaction tensors both strongly support the d_{xz}-d_{yz} type configuration for the unpaired electron on which the results in Table 3 are based.

A third possibility was tried, namely that the iron atom may be below the porphyrin plane, rather than on it, as assumed in the present work. However, taking the iron atom at a position as much as 0.23 Å below the porphyrin plane (by analogy with the metmyoglobin system [24a]) does not change the A_{zz} for the porphyrin nitrogens drastically, with the new values still less than 1 MHz. The A_{zz} for N_α and N_γ atoms of the azide group reduce in magnitude by about 18% still substantially larger than the experimental ^{14}N hyperfine constants [2]. In any case, as mentioned earlier, the ^{15}N substitution measurements [2] argue against the association of the experimental hyperfine constants with the azide nitrogens. These results thus show that the difference between the experimental and theoretical values of the hyperfine constants A_{zz} for the prophyrin nitrogens also cannot be resolved by the possibility of the iron atom position being off the porphyrin plane. This brings us then to the question of exchange polarization (EP) effect [24] which has not been included in the contact and dipolar contributions. From calculations on atomic systems [25], the ECP contribution to the dipole effect is expected to be rather small. The major focus therefore has to be on the EP contribution to the contact contribution A_F. One can include this effect partially through the use of semi-empirical formulae [35] that have been devised to incorporate EP contributions from π-type unpaired spin-distributions on the nitrogen atom and adjacent carbon atoms. To examine the importance of EP effects for pyrrole nitrogens, we have used one of these available formulae [35a] in the literature, based on the study of pyrazine free radicals, which leads to:

$$A_{\mathrm{ECP}} = (S^{\mathrm{N}} + 2Q^{\mathrm{N}}_{\mathrm{NC}})\rho^{\mathrm{N}} + 2Q^{\mathrm{N}}_{\mathrm{CN}}\rho^{\mathrm{C}} \tag{47}$$

ρ^{N} and ρ^{C} being the unpaired spin populations on the nitrogen atom and adjacent carbon atoms and $(S^{\mathrm{N}} + 2Q^{\mathrm{N}}_{\mathrm{NC}})$ and $2Q^{\mathrm{N}}_{\mathrm{CN}}$ are (86.60 ± 5.60) MHz and (5.6 ± 5.6) MHz respectively. Using this formula in conjunction with the unpaired spin populations for the configuration with the unpaired spin electron in a state involving a mixture of d_{xz} and d_{yz} symmetries, from our electronic structures results, one obtains values of A_{ECP} of 0.15, 0.24, 0.54 and 0.42 MHz for the porphyrin atoms N_2, N_3, N_4, and N_5 in Fig. 1. When these results are combined with the direct contributions results for A_{zz} in Table 3, one obtains for the net A_{zz} of the four porphyrin nitrogens, the values 0.44, 0.64, 1.36 and 1.09 MHz respectively. There is thus an improvement in the right direction for agreement with experiment [2] but not sufficient to bridge the substantial gap between theory and experiment.

The major remaining cause for the difference between theory and experiment

could be the influence of the EP effect of the substantial unpaired spin population on iron atom, about 63% of the net unpaired population in the molecule, which has not been included. To study this effect, one would need to carry out spin-polarized Hartree–Fock investigations [15a, 36] with different wave-functions for the paired spin states with opposite spin. It would be most satisfying to carry out first-principle Hartree–Fock calculations, although this would be rather time-consuming for the size of the molecular system we are dealing with for AzidoMb. It would also be helpful in the future to carry out calculations by the approximate procedure involving the Slater free-electron type approximation [37] such as the Multiple-Scattering X_α procedure [29] to obtain an estimate of the possible importance of the exchange polarization contribution. An alternate procedure would be a perturbation approach, handling the difference in the exchange potentials experienced by the paired spin electrons in different spin states as a perturbation as has been done in the literature in small molecular systems by summing over excited states [38] or using a differential equation approach [39].

4. Conclusion

In summary, our analysis of the electronic structure and magnetic and hyperfine properties of AzidoMb shows that a configuration involving the presence of five electrons in iron d-like molecular orbitals and the unpaired electron in a mixture of d_{xz} and d_{yz} symmetry, as in the case [1c] of ferricytochrome c, satisfactorily explains the observed g-tensor from EPR experiments [4], the ^{57m}Fe nuclear quadrupole splitting from Mössbauer measurements [4] and ^{14}N nuclear quadrupole interaction from ENDOR measurements [2]. However for the ^{57m}Fe and ^{14}N magnetic hyperfine constants which have been measured [2, 3] by Mössbauer effect and ENDOR technique [40] respectively, there are sizeable differences between theory and experiment. In the case of ^{57m}Fe, where the exchange polarization effect [24] associated with the exchange interaction between the unpaired spin and paired spin electrons has been included and makes a sizeable contribution, we have demonstrated in related work [34] that the discrepancy between theory using the ground state configuration considered in this work and experiment is associated with the modification of the orbital contribution and the finite orbital contribution to the hyperfine field tensor produced when one includes spin-orbit effects. For the case of the ^{14}N magnetic hyperfine interaction, where the orbital unquenching is expected to be small due to the weakness of the spin-orbit interaction for nitrogen atoms, the difference is ascribed to the possibility of substantial contributions from the exchange polarization effect associated with the sizeable unpaired spin population on the iron atom. Methods for studying these effects are proposed. On the experimental side, it is hoped that the association [2] of the observed ENDOR results for the ^{14}N magnetic hyperfine to porphyrin nitrogens will be rechecked in view of the fact that all the other properties of these molecules agree well with theory. It is also hoped that experimental values will be available for the azide ^{14}N magnetic hyperfine constants to check the sizeable values predicted in this work for the two end

nitrogen atoms and further verify the assumed electronic configuration for the molecule.

Acknowledgement. The authors are grateful to Professor Charles P. Scholes for valuable discussions.

Appendix: Transformation relations associated with *g*- and hyperfine tensors

Equation (20) describes the effective hyperfine constant expected for AzidoMb when the magnetic field is applied in any arbitrary direction. We shall briefly describe here the derivation of Eq. (20). Although our interest here is specifically in AzidoMb, the Eqs. (20)–(23) are of general applicability whenever there are two distinct principal axes systems for the g- and A-tensors which are themselves different from the crystal axes (a, b and c axes of the monoclinic system in the case of azidoMb), along which magnetic fields are often applied in Mössbauer measurements [3c] for studying hyperfine interactions. For AzidoMb, as mentioned already in the text, these three sets of axes are in turn different from the heme-based axes in Fig. 1. We shall describe the crystal axes as well as the principal axes of the g and A tensors in terms of their orientations with respect to the heme based axes. Referring to the applied field as $\boldsymbol{H}_{\text{app}}$ with direction cosines l, m and n in the heme-based system in Fig. 1, the Hamiltonian describing the interaction of the spin $\boldsymbol{S}$ of the molecule with $\boldsymbol{H}_{\text{app}}$ is given by the spin-Hamiltonian term:

$$\mathcal{H}_{\text{Spin}} = \boldsymbol{S} \cdot \boldsymbol{H}_{\text{eff}}, \tag{A1}$$

where

$$\boldsymbol{H}_{\text{eff}} = \boldsymbol{g} \cdot \boldsymbol{H} = (g_{\alpha\alpha} l \boldsymbol{e}_\alpha + g_{\beta\beta} m \boldsymbol{e}_\beta + g_{\gamma\gamma} n \boldsymbol{e}_\gamma) \boldsymbol{H}_{\text{app}}, \tag{A2}$$

whose orientation is different from $\boldsymbol{H}_{\text{app}}$ because of the tensor nature of $\boldsymbol{g}$. In Eq. (A2), $g_{\alpha\alpha}$, $g_{\beta\beta}$ and $g_{\gamma\gamma}$ refer to the principal components of $\boldsymbol{g}$ and $\boldsymbol{e}_\alpha$, $\boldsymbol{e}_\beta$ and $\boldsymbol{e}_\gamma$ are the corresponding unit vectors along the principal axes. Thus the spin $\boldsymbol{S}$ of the molecule will align itself along a direction defined by the unit vector $\boldsymbol{e}_{\text{eff}}$ describing the direction of $\boldsymbol{H}_{\text{eff}}$, namely:

$$\boldsymbol{e}_{\text{eff}} = \left(\frac{g_{\alpha\alpha} l \boldsymbol{H}_{\text{app}}}{|\boldsymbol{H}_{\text{eff}}|}\right) \boldsymbol{e}_\alpha + \left(\frac{g_{\beta\beta} m \boldsymbol{H}_{\text{app}}}{|\boldsymbol{H}_{\text{eff}}|}\right) \boldsymbol{e}_\beta + \left(\frac{g_{\gamma\gamma} n \boldsymbol{H}_{\text{app}}}{|\boldsymbol{H}_{\text{eff}}|}\right) \boldsymbol{e}_\gamma, \tag{A3}$$

where the magnitude $|\boldsymbol{H}_{\text{eff}}|$ of $\boldsymbol{H}_{\text{eff}}$ is given by:

$$|\boldsymbol{H}_{\text{eff}}| = \sqrt{g_{\alpha\alpha}^2 l^2 + g_{\beta\beta}^2 m^2 + g_{\gamma\gamma}^2 n^2}\, \boldsymbol{H}_{\text{app}}. \tag{A4}$$

The effective hyperfine constant A_{eff} that would be observed in this situation is that corresponding to the component of the hyperfine field along the direction of $\boldsymbol{S}$. Thus,

$$A_{\text{eff}} = \boldsymbol{e}_{\text{eff}} \cdot \boldsymbol{A} \cdot \boldsymbol{e}_{\text{eff}}, \tag{A5}$$

where $\boldsymbol{A}$ is the hyperfine tensor with principal axes oriented along the unit vectors $\boldsymbol{e}_{\alpha'}$, $\boldsymbol{e}_{\beta'}$ and $\boldsymbol{e}_{\gamma'}$, the principal components and principal axes being determined from our theoretical investigations by the procedure described in Sect. 3.6. Using Eq (A6) for $\boldsymbol{A}$ namely:

$$\boldsymbol{A} = A_{\alpha'\alpha'} \boldsymbol{e}_{\alpha'} \boldsymbol{e}_{\alpha'} + A_{\beta'\beta'} \boldsymbol{e}_{\beta'} \boldsymbol{e}_{\beta'} + A_{\gamma'\gamma'} \boldsymbol{e}_{\gamma'} \boldsymbol{e}_{\gamma'}, \tag{A6}$$

where $A_{\alpha'\alpha'}$, $A_{\beta'\beta'}$ and $A_{\gamma'\gamma'}$ are the principal components of $\boldsymbol{A}$ and Eq. (A3) for $\boldsymbol{e}_{\text{eff}}$, one gets the relation

$$A_{\text{eff}} = A_{\alpha'\alpha'} l'^2 + A_{\beta'\beta'} m'^2 + A_{\gamma'\gamma'} n'^2 \tag{A7}$$

with

$$l' = (e_{\text{eff}} \cdot e_{\alpha'}), \qquad m' = (e_{\text{eff}} \cdot e_{\beta'}), \qquad n' = (e_{\text{eff}} \cdot e_{\gamma'}). \tag{A8}$$

Equations (A7) and (A8) correspond to Eqs. (20) and (21) in Sect. 2.4.

References and notes

1. (a) Mun SK, Chang JC, Das TP (1979) Proc Natl Acad Sci USA 76:4842
   (b) Mishra SL (1981) PhD Thesis, State University of New York at Albany
   (c) Mishra KC, Mishra SK, Das TP (1983) J Am Chem Soc 105:7729
2. Mulks CF, Scholes CP, Diskinson LC, Lapidot A (1979) J Am Chem Soc 101:1645
3. (a) Lang G, Marshall W (1966) Proc Phys Soc 87:3
   (b) Rhynard D, Lang G, Spartalian K, Yonetani T (1979) J Chem Phys 71:3715
   (c) Harami T (1979) J Chem Phys 71:1309
4. (a) Dickinson LC, Chien JCW (1977) J Biol Chem 252:1327
   (b) Helcke' GA, Ingram DJE, Slade EF (1968) Proc Roy Soc B169:275
   (c) Hori H (1971) Biochem Biophys Acta 251:277
   (d) See Helcke' et al [4b]. From the data in Table I of Hori [4c], assuming that the heme planes in azido and met Mb coincide, the angle between the largest component of g and the heme normal comes out as 8°, close to the value of 9° in [4b]
5. (a) Zerner M, Gouterman M, Kobayashi H (1966) Theor Chim Acta 6:363
   (b) Han PS, Das TP, Rettig MF (1970) Theor Chim Acta 16:1
6. Stryer L, Kendrew JC, Watson HC (1964) J Mol Biol 8:96
7. Weissbluth M (1974) In: Hemoglobin, chap 2. Springer, New York–Heidelberg–Berlin; Takano T (1977) J Mol Biol 110:537; Chien JCW (1969) J Chem Phys 51:4220; Peisach J, Blumberg W, Adler A (1973) Ann NY Acad Sci 206:310
8. (a) Trautwein A, Zimmermann R, Harris F (1975) Theor Chim Acta 37:89
   (b) Loew G, Kirchner RF (1975) J Am Chem Soc 97:7388; Loew G (1978) Biophys J 22:179
9. Mallick MK, Chang JC, Das TP (1978) J Chem Phys 68:1462
10. Huynh BH, Case DA, Karplus M (1977) J Am Chem Soc 99:6103
11. Case DA, Huynh BH, Karplus M (1979) J Am Chem Soc 101:4433
12. Dedieu A, Rohmer MM, Veillard A (1976) In: Proceedings of the 9th Jerusalem Symposium on Quantum Chemistry and Biochemistry, March 1976, Metal Ligand Interactions in Organic Chemistry and Biochemistry; Dedieu A, Rohmer MM, Bernard M, Veillard A (1976) J AM Chem Soc 98:3717
13. Han PS, Rettig MF, Das TP (1970) Theor Chem Acta 16:1; Han PS, Rettig MF, Das TP (1972) J Chem Phys 56:3686; Mun SK, Mallick MK, Mishra SL, Chang JC, Das TP (1981) J Am Chem Soc 103:5024; Mallick MK, Mun SK, Mishra SL, Chang JC, Das TP (1978) Hyperfine Interact 4:914; Chang JC, Kim YM, Das TP (1975) J Chem Phys 67:4350; Mun SK, Chang JC, Das TP (1977) Biochem Biophys Acta 490:249, Mishra SL, Chang JC, Das TP (1980) J Am Chem Soc 102:2674
14. The SCCEH calculations by Loew G and Kirchner RF (1975) [8], leads to a ^{57m}Fe quadrupole coupling constant of −1.81 mm/sec when one uses the recent value of the quadrupole moment of ^{57m}Fe of 0.082 barns (Ref. [15]) in satisfactory agreement with the experimental value of −2.11 mm/s. (See Spartalin K, Lang G (1976) J Phys Colloq C6 37:195)
15. (a) Duff KJ, Mishra KC, Das TP (1981) Phys Rev Lett 46:1611
   (b) Vajda S, Sprouse GD, Rafailovich MH, Noe JW (1981) Phys Rev Lett 47:1230
   (c) Watson RE, Sternheimer RM, Bennett LH (1984) Phys Rev B 30:5209
16. Mulliken RS (1955) J Chem Phys 23:1833
17. (a) Peisach J, Blumberg WE, Adler A (1973) Ann NY Acad Sci 206:310
   (b) Chien JCW (1969) J Chem Phys 51:4220
   (c) Doetschman DC, Utterback SG (1981) J Am Chem Soc 103:2847
18. Mishra KC, Mishra SK, Roy JN, Ahmad S, Das TP (1985) J Am Chem Soc 107:7898
19. Carrington A, McLachlan AD (1963) In: Introduction to magnetic resonance, chap 9. Harper and Row, New York

20. Das TP (1973) In: Relativistic quantum mechanics of electrons, chap 7. Harper and Row, New York
21. Das TP, Hahn EL (1958) In: Nuclear quadrupole resonance spectroscopy. Solid State Physics Supplement, vol 1. Academic Press, New York
22. Chang JC, Ikenberry D, Das TP (1974) Theor Chim Acta 35:361
23. Ray SN, Das TP (1977) Phys Rev B16:4794
24. (a) Mun SK, Chang JC, Das TP (1979) J Am Chem Soc 101:5562
    (b) Mallick MK, Chang JC, Das TP (1978) J Chem Phys 68:1462
    (c) Mallick MK, Mun SK, Mishra SL, Chang JC, Das TP (1978) Hyperfine Interact 4:914
25. (a) McConnell HM (1956) J Chem Phys 24:764
    (b) Chang SY, Davidson ER, Vincow G (1968) J Chem Phys 49:529, Chang SY, Davidson ER, Vincow G (1970) 52:1740
    (c) Rodgers JE, Lee T, Das TP, Ikenberry D (1973) Phys Rev A7:51
    (d) Lyons JD, Pu RT, Das TP (1969) Phys Rev 178:103
    (e) Sternheimer RM (1952) Phys Rev 86:1
26. Dickinson LC et al. in [4]
27. Mun SK, Mallick MK, Mishra SL, Chang JC, Das TP (1981) J Am Chem Soc 103:5024
28. (a) Duff KJ, Mishra KC, Das TP (1981) Phys Rev Lett 46:1611
    (b) Herman K, Bagus PS (1979) Phys Rev B20:1603
29. Johnson KH (1973) Adv Quantum Chem 7:143
30. (a) Das TP in [20]
    (b) Rao BK, Ikenberry D, Mahanti SD, Gaspari GD, Das TP (1969) J Magn Reson 1:221
    (c) Ikenberry D, Jette AN, Das TP (1970) Phys Rev B1:2875
    (d) Ikenberry D, Das TP (1970) Phys Rev B1:1219
    (e) McConnell HM in [13]
31. (a) Das TP in [10]
    (b) Evans L, Sandars PGH, Woodgate GK (1965) Proc Roy Soc A289:108, 114
    (c) Andriessen J, Raghunathan K, Ray SN, Das TP (1977) Phys Rev B15:2533
    (d) Andriessen J, Van Ormondt D, Ray SN, Das TP (1978) J Phys B11:2601
32. (a) McNab TK, Carsten DHW, Gruen DM, McBeth RL (1972) Chem Phys Lett 13:600
    (b) Litterst FJ, Schichl A, Kalvius GM (1978) Chem Phys 28:29
33. Lang G, Dale BW (1973) J Phys C 6:L80, Rhynard D, Lang G, Spartalian K, Yonetani T (1979) J Chem Phys 71:3715
34. Roy JN, Mishra SK, Mishra KC, Das TP Chem Phys, in press
35. See for instance
    (a) Stone EW, Maki AH (1963) J Chem Phys 39:1635
    (b) Karplus M, Fraenkel GK (1961) J Chem Phys 35:1312
36. Watson RE, Freeman AJ (1971) In: Freeman AJ, Fraenkel RB (ed) Hyperfine interactions. Academic Press, New York, p 53
37. Das TP, in [20]
38. Rodgers JE, Lee T, Das TP, Ikenberry D (1973) Phys Rev A7:51, Kristiansen P, Veseth L (1986) J Chem Phys 84:2711
39. Bernheim RA, Das TP (1960) J Chem Phys 33:1813
40. Feher G (1959) Phys Rev 114:1219